Mech. Sci., 17, 333–346, 2026
https://doi.org/10.5194/ms-17-333-2026

Mechanical Sciences
Open Access

Analysis of sensitive wavelengths in railway vehicles with different inerter-based suspension systems

Dilai Chen[1], Chunli Liu[1], Zhanghui Xia[2], Gengchen Sun[3], Rang Zhang[1], and Rui Song[4,5]

[1]School of Rail Transportation, Shanghai Institute of Technology, Shanghai 201418, China
[2]Locomotive & Car Research Institute, China Academy of Railway Sciences Corporation Limited, Beijing 100081, China
[3]Department of Information Engineering, Taishan Polytechnic, Taian 271001, China
[4]China Railway Test & Certification Center Co., Ltd., Beijing 100081, China
[5]Standards and Metrology Research Institute, China Academy of Railway Sciences Corporation Limited, Beijing 100081, China

Correspondence: Rang Zhang (zhangrang@sit.edu.cn)

Received: 8 October 2025 – Revised: 16 January 2026 – Accepted: 25 February 2026 – Published: 25 March 2026

Abstract. To enhance the dynamic performance and stability of high-speed railway vehicles, this study investigates the vibration attenuation mechanism of the transverse secondary inertial suspension System (TSISS). Based on vehicle–track coupled dynamics, models were established for a conventional suspension (Condition S1: parallel spring–damper) and four TSISS configurations (Condition S2: parallel inerter–spring–damper); an inerter in series with a damper, parallel to the air spring (Condition S3); an inerter in series with a spring, parallel to the air spring–damper (Condition S4); and a parallel spring–damper unit in series with an inerter, all parallel to the air spring (Condition S5). The analysis focuses on the response distribution of sensitive wavelengths under track irregularity excitations and their impact on ride comfort. Results indicate distinct frequency domain characteristics: Conditions S2 and S4 show sensitivity to short wavelengths (peaking around 20 m), improving ride quality indices by 11 % and 8 % over S1, respectively. Conversely, Conditions S3 and S5 target the longwave range, yielding improvements of 14 % and 28 %. Validated by coherence function analysis, Condition S5 significantly suppresses longwave irregularities (40–150 m), with a response peak near 105 m. Notably, with inertance set between 500 and 1000 kg, Condition S5 achieves a ride quality index of approximately 2.75 and substantially reduces lateral acceleration, demonstrating superior ride comfort.

1 Introduction

As high-speed railway networks expand, running stability and ride comfort have become critical performance metrics (Xu et al., 2020; Zhu et al., 2021). Track irregularities impose complex excitations, among which specific "sensitive wavelengths" significantly govern ride quality (Tian, 2015). Traditional passive suspensions, constrained by fixed parameters, struggle to adapt to these variable spectra. Consequently, the inerter has emerged as a promising solution for suspension systems (Chen and Zhu, 2021). Inerters exhibit significant low-frequency attenuation capabilities. Integrated into high-speed railway suspensions, they suppress car body vibrations and enhance stability; however, their efficacy relies heavily on precise topological configuration and parameter tuning (Wang, 2023; Qi et al., 2025a). Despite these advances, existing research largely treats the inerter in isolation, overlooking the intrinsic correlation between track irregularity excitations and suspension system responses. Specifically, a systematic analysis of how distinct inerter configurations influence the response to sensitive wavelengths remains absent.

Lateral vibration, primarily induced by track alignment irregularities and curve negotiation, is a dominant factor affecting ride comfort (Liu, 2023). Incorporating inerters into the secondary lateral suspension can suppress low- to medium-frequency swaying without substantially increasing unsprung mass. To evaluate this performance, accu-

Table 1. Degrees of freedom of the vehicle model.

No.	Component	Longitudinal	Lateral	Vertical	Roll	Pitch	Yaw
1	Wheelsets (4)	√	√	√	√	√	√
2	Axle boxes (8)					√	
3	Bogies (2)	√	√	√	√	√	√
4	Car body	√	√	√	√	√	√

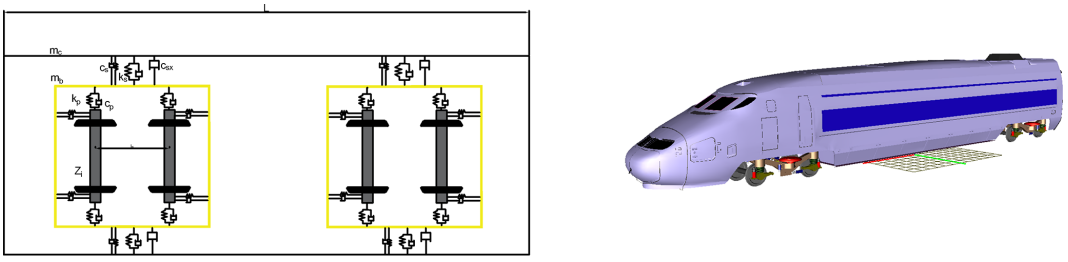

(a) (b)

Figure 1. **(a)** Topological structure of the railway vehicle. **(b)** Schematic diagram of the overall vehicle dynamics model.

rate vehicle–track coupled modeling is essential. Dižo et al. (2019) investigated wagon multibody system fundamentals, emphasizing precise component modeling to capture realistic dynamic responses. Sowiński et al. (2021) further demonstrated that geometric variations, such as rail inclination and profile wear, significantly alter wheel–rail contact conditions. Moreover, Kostrzewski and Melnik (2021) identified model-based simulation as a pivotal trend for validating monitoring data and predicting vehicle behaviors, a practice exemplified by Chudzikiewicz (2017). Regarding wavelength sensitivity, Yu et al. (2016) identified critical ranges via system input–output analysis. Chen et al. (2025), utilizing power spectral density and coherence analysis on passenger and freight cars, pinpointed 40–150 m as the unfavorable wavelength range impacting high-speed operations. Furthermore, Qi et al. (2025b) observed a linear relationship between irregularity amplitude and dynamic response, and Sun et al. (2022) proposed vibration absorbers to mitigate these instability factors.

Since Smith (2002) introduced the inerter – defined by force output proportional to relative acceleration – its application has expanded significantly. Zhuang et al. (2019) demonstrated that inerter–spring–damper (ISD) systems effectively suppress seismic responses in structural isolation. In vehicle dynamics, Sharma et al. (2023a, b) highlighted the potential of intelligent semi-active suspensions (e.g., ANFIS based), reporting ride comfort improvements of 8.19 %–31.50 % over passive counterparts. However, these studies predominantly address free vibration or harmonic excitation; the response characteristics and wavelength sensitivity of inerters under realistic, wide-wavelength track irregularities remain insufficiently explored.

This study investigates the sensitive-wavelength distribution of the transverse secondary inertial suspension system (TSISS). Given that secondary suspensions govern car body stability, the research focuses on the lateral inerter mechanism to provide a theoretical basis for optimizing ride comfort in high-speed trains.

2 Dynamic modeling and simulation of railway vehicles under different suspension conditions

To accurately capture lateral vibration characteristics under track irregularity excitations, a high-fidelity multibody dynamics model of the CRH3 EMU cab car was established utilizing Universal Mechanism (UM) software. By evaluating acceleration responses across various inerter suspension configurations, this study screens for the topology yielding superior dynamic performance, thereby establishing a baseline for the subsequent investigation of sensitive wavelengths.

2.1 Establishment of the vehicle dynamics model

The vehicle is modeled as a complex system comprising 15 rigid bodies: one car body, two bogie frames, four wheelsets, and four axle boxes (represented by eight distinct components). The system features a total of 50 degrees of freedom (DOFs), with the specific distribution detailed in Table 1. The model explicitly accounts for the vehicle's topological structure, incorporating precise representations of the primary suspension, the secondary suspension (integrating the transverse secondary inertial suspension system, TSISS), and nonlinear wheel–rail contact geometry. This high-fidelity framework effectively captures dynamic responses under op-

Table 2. Parameters of the railway vehicle.

No.	Parameter description	Symbol	Parameter values	Unit
1	Mass of car body	m_c	30	t
2	Mass of bogie frame	m_b	2.5	t
3	Primary suspension stiffness	k_p	2000	kN m^{-1}
4	Primary suspension damping	c_p	240	(kN s) m^{-1}
5	Secondary suspension stiffness	k_s	360	kN m^{-1}
6	Secondary suspension damping	c_s	16	(kN s) m^{-1}
7	Damping of yaw damper	c_{sx}	150	(kN s) m^{-1}
8	Wheelbase	l_w	2.5	m
9	Vehicle length	L	25	m
10	Vertical displacement of wheelset	$Z_{wi}(i = 1–4)$	2.2	m
11	Stiffness of vibration reduction spring	k_b	200	kN m^{-1}

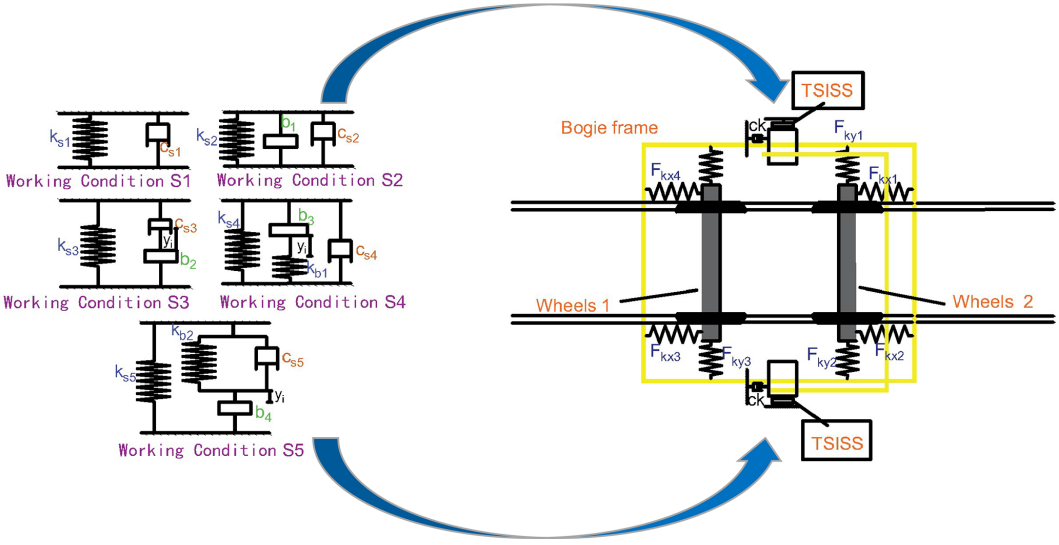

Figure 2. Different configurations of secondary inerter-based suspension systems.

erational conditions, serving as a reliable numerical benchmark for the subsequent comparative analysis of suspension configurations.

Figure 1a illustrates the vehicle topology, with corresponding nomenclature detailed in Table 2. A bottom-up modeling approach was employed: wheelsets were established as fundamental subsystems and integrated into the bogie frame to form the bogie assembly. These subsystems were then coupled with the car body to complete the full-vehicle dynamics model, as shown in Fig. 1b. This hierarchical procedure accurately captures the kinematic constraints among components, providing a robust foundation for subsequent dynamic simulations and control algorithm integration.

While the comprehensive multibody model serves as the baseline for numerical simulation, a simplified analytical model was derived to elucidate the vibration attenuation mechanism of the TSISS. This reduced-order model facilitates efficient parametric analysis, particularly regarding frequency domain sensitivity to track irregularities.

Assuming small-amplitude oscillations, the system was linearized and reduced to its essential degrees of freedom (DOFs). The model specifically captures the lateral and roll motions of the car body coupled with the lateral displacements of the front and rear bogies. This configuration effectively isolates the interaction between the car body and the secondary lateral suspension. To ensure validity, all physical parameters – including mass, inertia, stiffness, damping, and inertance – remain consistent with those in the high-fidelity multibody model.

2.2 Configuration design of inerter suspension systems

Analogous to springs and dampers, the inerter is a two-terminal mechanical element where the generated force is proportional to the relative acceleration between its terminals. The integration of an inerter can effectively attenuate

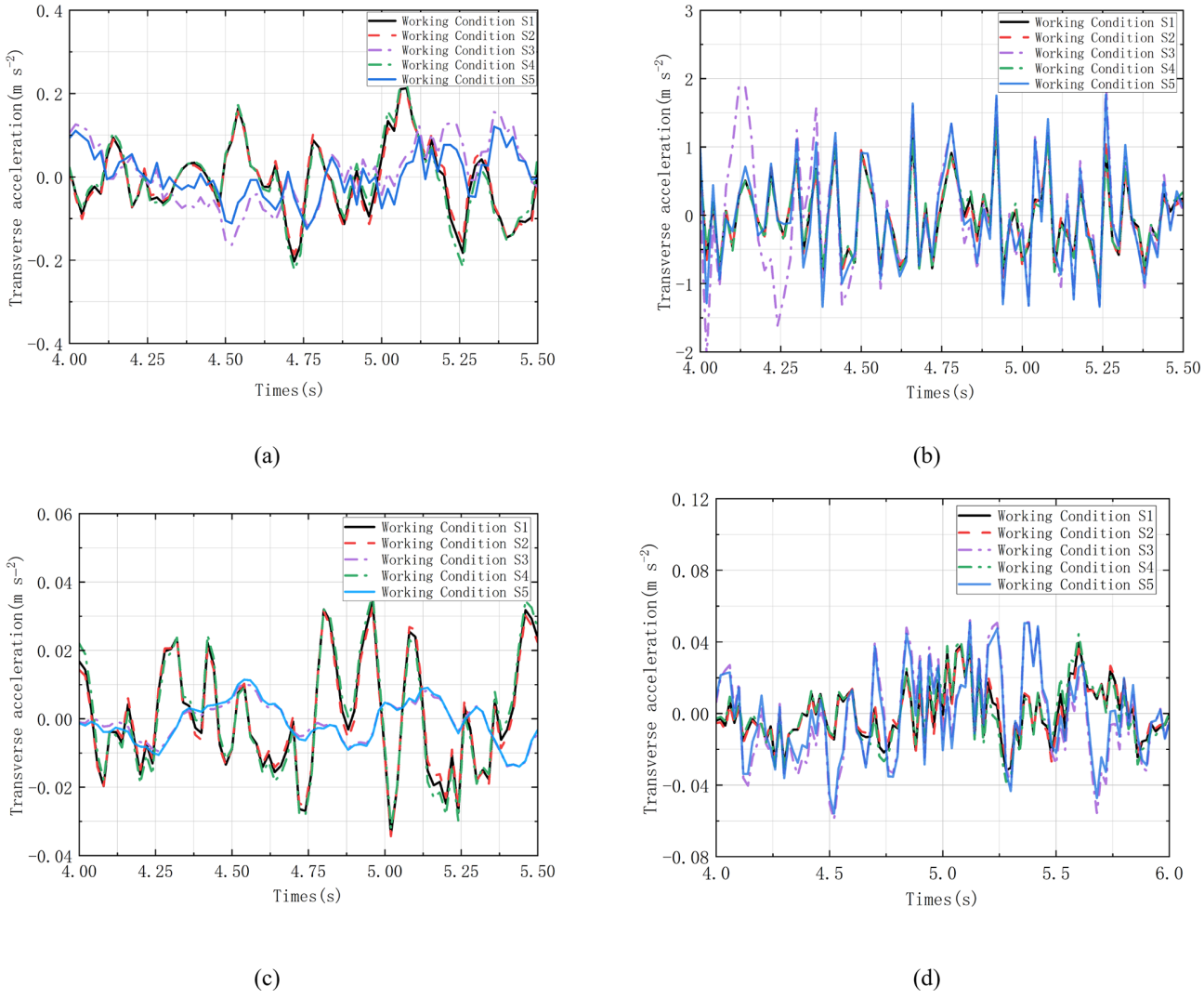

Figure 3. **(a)** Lateral car body acceleration. **(b)** Lateral acceleration of the bogie frame. **(c)** Car body yaw acceleration. **(d)** Car body roll acceleration.

vibration acceleration amplitudes and extend the oscillation period, thereby theoretically enhancing the running stability of railway vehicles. The constitutive equation of the inerter is expressed as Eq. (1):

$$F = b\frac{\mathrm{d}(v_1 - v_2)}{\mathrm{d}t}, \tag{1}$$

where F is the force applied to the two terminals of the inerter (unit: N), b is the inertance (unit: kg), and v_1 and v_2 denote the accelerations of the two terminals (unit: m s^{-1}).

Drawing on optimization studies by Wang et al. (2022), several inerter configurations were selected to investigate their impact on sensitive-wavelength distribution under lateral excitations. The inerter models were integrated into the vehicle system by modifying the dynamic stiffness matrices. To accurately simulate series topologies, a virtual mass block was introduced as an intermediate node between the inerter and other suspension elements; this ensures consistency between the numerical simulation and theoretical formulation. The schematics of the conventional secondary lateral suspension and the four proposed inertial configurations are presented in Fig. 2.

In Fig. 2, F_{kyi} and F_{kxi} $(i = 1\text{–}4)$ represent the primary lateral stiffness and primary longitudinal stiffness(unit: kN m^{-1}), respectively; b_i $(i = 1\text{–}4)$ denotes the inertance (unit: kg); and k_{bi} $(i = 1, 2)$ represents the stiffness of the vibration reduction spring in the suspension systems of Conditions S4 and S5.

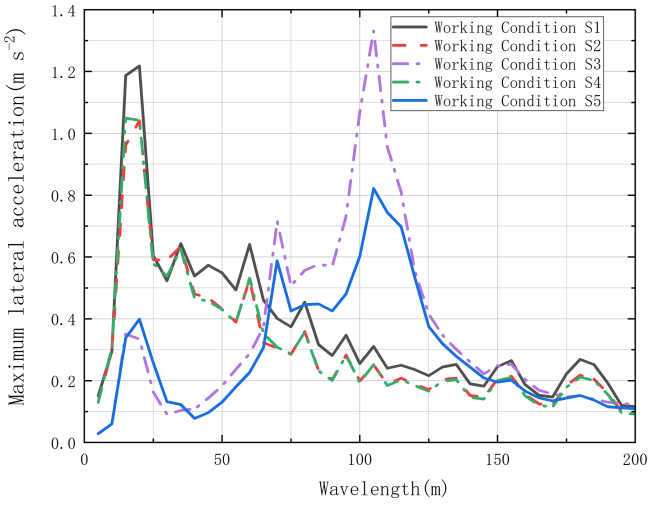

Figure 4. Distribution of sensitive wavelengths of railway vehicle lateral irregularities under different suspension cases.

The dynamic equations for Conditions S1 through S5 correspond to Eqs. (2)–(6), respectively.

$$m_c\ddot{y}_c + k_{s1}(y_c - y_b) + c_{s1}(\dot{y}_c - \dot{y}_b) = 0, \tag{2}$$

$$m_c\ddot{y}_c + b_1(\ddot{y}_c - \ddot{y}_b) + k_{s2}(y_c - y_b) + c_{s2}(\dot{y}_c - \dot{y}_b) = 0, \tag{3}$$

$$\begin{cases} m_c\ddot{y}_c + k_{s3}(y_c - y_b) + c_{s3}(\dot{y}_c - \dot{y}_i) = 0, \\ c_{s3}(\dot{y}_c - \dot{y}_i) = b_2(\ddot{y}_i - \ddot{y}_b) \end{cases} \tag{4}$$

$$\begin{cases} m_c\ddot{y}_c + c_{s4}(\dot{y}_c - \dot{y}_b) + k_{s4}(y_c - y_b) + k_{b1}(y_c - y_i) = 0, \\ k_{b1}(y_c - y_i) = b_3(\ddot{y}_i - \ddot{y}_b) \end{cases} \tag{5}$$

$$\begin{cases} m_c\ddot{y}_c + k_{s5}(y_c - y_b) + k_{b2}(y_c - y_i) + c_{s5}(\dot{y}_c - \dot{y}_i) = 0, \\ k_{b2}(y_c - y_i) + c_{s5}(\dot{y}_c - \dot{y}_i) = b_4(\ddot{y}_i - \ddot{y}_b) \end{cases} \tag{6}$$

Here y_c denotes the lateral displacement of the car body, and y_b denotes the lateral displacement of the bogie frame. Furthermore, y_i represents the lateral displacement of the virtual mass block, which is introduced to implement the series connection between the inerter and the damper in the model comprising the car body m_c and the bogie frame m_b.

2.3 Analysis of the influence of inerter-based systems on vehicle dynamics

Lateral car body acceleration is a critical metric for assessing vehicle running stability (Qi et al., 2025a). To investigate the efficacy of different inerter-based suspension systems, numerical simulations were performed using a measured domestic track irregularity spectrum as the excitation source. The evaluation focused on lateral accelerations of the car body and bogie frame, along with car body yaw and roll accelerations. In these simulations, the inertance was fixed at 500 kg, and the operating speed was set to 250 km h^{-1}. The corresponding response characteristics are illustrated in Fig. 3.

Lateral Car Body Acceleration (Fig. 3a). Trends for Conditions S2 and S4 mirror the baseline Condition S1, with similar peak amplitudes, indicating negligible improvement. In contrast, Conditions S3 and S5 demonstrate significant suppression. Specifically, Condition S5 reduces the peak acceleration to 0.21 m s^{-2} – an optimization of 34 % relative to S1. This confirms the inerter system's capability to effectively attenuate vibration through an energy redistribution mechanism.

Lateral Bogie Frame Acceleration (Fig. 3b). While S2 and S4 again remain consistent with S1, Condition S3 exhibits pronounced fluctuations during the initial 4.5 s, showing no clear benefit. Notably, Condition S5 results in a slight deterioration (7 % increase) compared to S1. This indicates a trade-off: the inerter suppresses car body vibration by transferring partial energy to the bogie subsystem. Consequently, dynamic performance optimization alters energy transmission paths, necessitating multi-objective optimization for specific performance indices in engineering practice.

Car body yaw acceleration (Fig. 3c). Conditions S2 and S4 show no significant deviation from S1. Conversely, compared to the baseline, Conditions S3 and S5 achieve substantial reductions of 31 % and 34 %, respectively. The response of S5 fluctuates near 0 m s^{-2}, indicating that the "parallel damper–spring, series inerter, parallel air spring" topology effectively mitigates yaw motion without inducing resonance in this degree of freedom.

Car body roll acceleration (Fig. 3d). S2 and S4 exhibit trends consistent with S1. However, Conditions S3 and S5 show slight performance degradation relative to S1. This is attributed to the series inerter configuration in these cases, which alters system coupling and slightly compromises the balance of multi-degree-of-freedom vibration suppression.

Comparative analysis of Fig. 3 demonstrates that the introduction of inerter systems induces distinct modulation characteristics in vehicle dynamics. Notably, Condition S5 effectively mitigates lateral car body acceleration, particularly under longwave track irregularities. While this suppression involves transferring vibrational energy to the bogie subsystem – raising lateral frame acceleration to approximately 1.5 m s^{-2} – the resulting value remains significantly below the safety threshold of 8 m s^{-2} mandated by the GB/T 5599-2019 standard. Consequently, leveraging composite structures to enhance frequency band adaptability presents a promising approach for optimizing both ride quality and running stability.

3 Analysis of sensitive-wavelength distribution characteristics

The preceding analysis confirms that Condition S5 significantly reduces lateral car body acceleration at 250 km h^{-1}. However, the concomitant impact on bogie frame vibration suggests that the suspension's attenuation efficacy is closely correlated with the wavelength characteristics of track irregularities. To elucidate the system's wavelength adaptability,

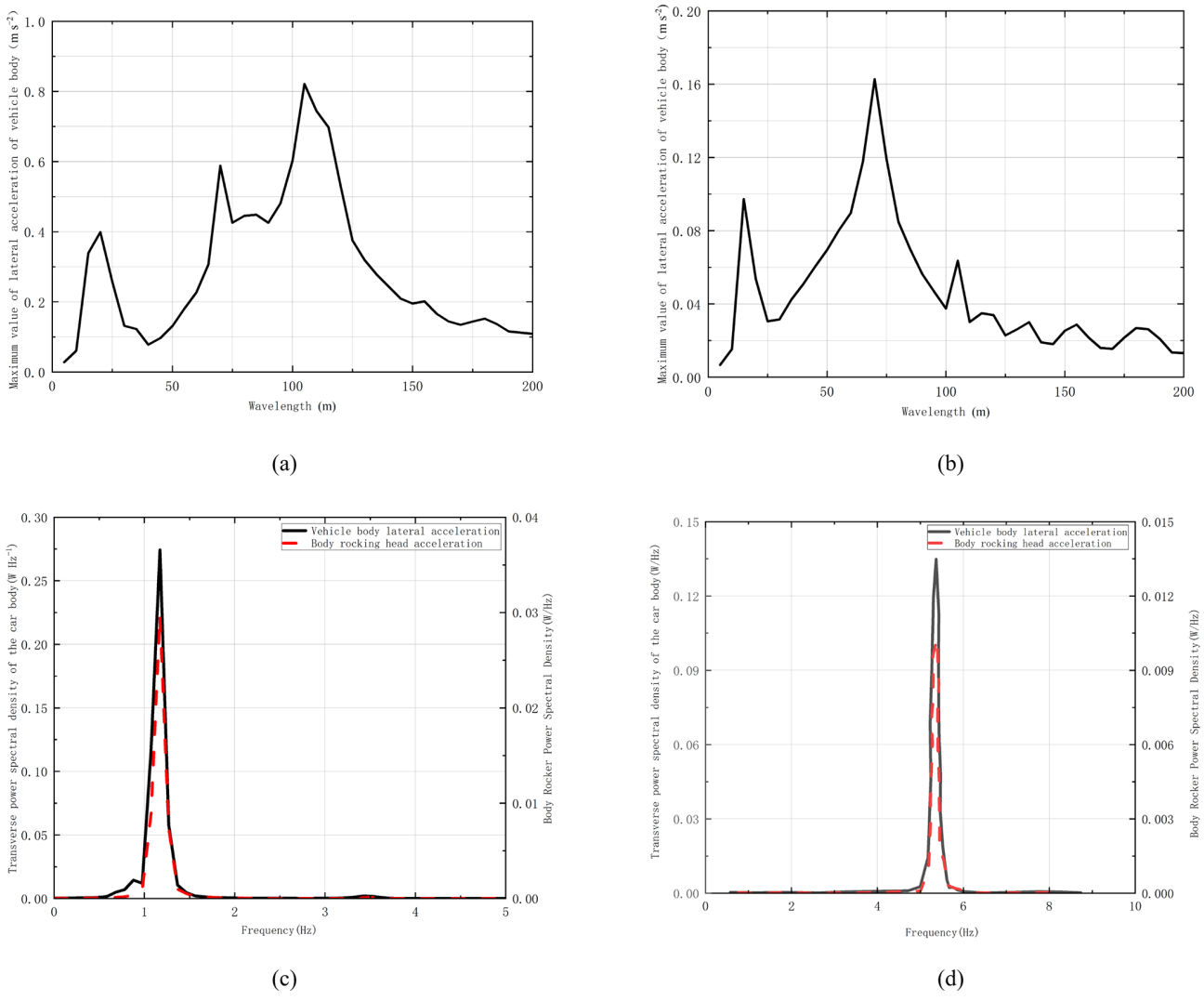

Figure 5. **(a)** Sensitive wavelengths of car body lateral vibration. **(b)** Sensitive wavelengths of car body yaw vibration. **(c)** Frequency domain analysis at 15 m wavelength. **(d)** Frequency domain analysis at 70 m wavelength.

the following section investigates the distribution of sensitive wavelengths across varying suspension configurations, operating speeds, and inertance coefficients.

3.1 Influence of suspension configurations

Considering the weak coupling between vertical and lateral vibrations in railway vehicles (Sun et al., 2024), measured vertical irregularities were incorporated to ensure simulation fidelity without compromising the lateral analysis. Conversely, to systematically isolate the effects of wavelength and amplitude, lateral irregularities were modeled as harmonic excitations. The simulation covered a wavelength range of 5–200 m (5 m increments) with a fixed amplitude of 4 mm, at a constant vehicle speed of 250 km h^{-1}. The peak lateral car body acceleration served as the primary metric for identifying the sensitive-wavelength distribution.

As shown in Fig. 4, S1, S2, and S4 exhibit dominant responses in the short-wavelength regime, peaking around 20 m. Compared to the baseline (S1), S2 and S4 attenuate peak accelerations by 16.1 % and 13.3 %, respectively. In contrast, S3 and S5 shift the sensitive range to long wavelengths ($\sim$ 105 m), with S5 achieving the most significant suppression of 32.2 %. These findings substantiate that integrating inerters into the suspension system significantly enhances lateral dynamic performance.

To investigate the minor local peaks observed in Condition S5's lateral acceleration at wavelengths of 70 and 15 m (Fig. 4), further analysis was conducted, as shown in Fig. 5. Corresponding peaks are also evident in the car body yaw motion (Figs. 5a and 6b). Power spectral density (PSD) analysis (Fig. 5c and d) reveals that under 70 m excitation, the dominant frequency for both lateral and yaw modes coincides at 1.17 Hz. Similarly, under 15 m excitation, the domi-

nant frequencies are highly proximal (5.3 and 5.5 Hz, respectively). This frequency alignment implies that the local peaks in lateral acceleration stem from a resonant coupling between lateral and yaw motions, a phenomenon corroborated by recent studies (Alves et al., 2023; Jiang et al., 2022).

3.2 Influence of running speed

The influence of running speed (250–350 km h^{-1}) on sensitive-wavelength distribution was investigated under harmonic lateral track irregularity excitations (Jiang et al., 2022; Wei and Xu, 2021). As illustrated in Fig. 6, the distribution pattern of sensitive wavelengths remains substantially stable across all suspension configurations, demonstrating insensitivity to speed variations. However, regarding amplitude, the maximum lateral car body accelerations for Conditions S2, S4, and S5 exhibit a distinct upward trend as speed increases.

In Condition S3, a counterintuitive phenomenon occurs under specific excitation wavelengths: maximum lateral car body acceleration decreases as vehicle speed increases. Combined time–frequency analysis (Fig. 7) reveals that this anomaly arises from the interaction between multi-degree-of-freedom modal coupling and phase modulation mechanisms.

Specifically, at 270 km h^{-1} (Fig. 7a and c), resonant coupling between car body lateral and roll modes near 0.78 Hz amplifies the lateral acceleration. Conversely, at 380 km h^{-1} (Fig. 7b and d), although the dominant frequencies of roll and yaw motions converge near 1 Hz, their time-domain waveforms exhibit anti-phase characteristics. Consequently, the lateral response is significantly attenuated via destructive interference (or vibration energy cancellation) (Li and Xu, 2022). These findings demonstrate that the sensitive-wavelength distribution of the inerter suspension is governed not merely by the speed–wavelength mapping, but also significantly by complex multi-DOF modal interactions.

3.3 Influence of inertance coefficient

The selection of an optimal inertance coefficient is critical for the suspension system's vibration attenuation efficiency. Preliminary frequency domain analysis indicates that an inertance range of 10^2–10^3 kg is required to effectively shift the car body's dominant lateral frequency away from the sensitive band. Furthermore, based on existing mechanical designs, inertance coefficients between 500 and 2000 kg can be readily accommodated within the spatial constraints of the vehicle's secondary suspension (Chen et al., 2022).

Figure 9 depicts the maximum lateral car body acceleration as a function of track irregularity wavelength and inertance coefficient (b). Cases S2 through S4 exhibit negligible sensitivity to parameter variations, with peak fluctuations remaining below 5 % and showing no discernible trend. Conversely, Case S5 demonstrates a pronounced dependence on inertance. Specifically, increasing b from 500 to 1000 kg reduces the peak acceleration at $\sim$ 105 m from 0.85 to 0.55 m s^{-2} – a significant 35.3 % improvement. This confirms the system's efficacy in suppressing longwave excitations within this specific range. However, further increasing b from 1000 to 2000 kg yields marginal returns (reduction < 5 %), indicating that vibration attenuation performance has reached saturation. This indicates that the inerter suspension system in Condition S5 plays a positive role in vibration attenuation. An inertance within the range of 1000 kg balances dynamic performance with engineering feasibility, thereby providing a basis for parameter design.

4 Analysis of ride quality

This section evaluates the influence of different inerter suspension configurations on the vehicle's dynamic performance, specifically focusing on ride comfort. First, the assessment methodology based on the Sperling index (GB/T 5599-2019) is introduced to quantify lateral vibration characteristics. Subsequently, the ride quality indices of the proposed TSISS configurations are analyzed under varying track irregularity wavelengths and vehicle speeds to ultimately identify the configuration yielding the optimal ride quality index.

The vehicle ride quality is quantitatively assessed in accordance with the GB/T 5599-2019 standard. This standard employs the Sperling index (W), which characterizes lateral and vertical vehicle vibrations by incorporating a human perception filter and frequency-weighted energy distribution. The widespread adoption of the Sperling index by major entities, including the European Union Agency for Railways (ERA) and CRRC, underscores its engineering applicability and robustness.

Specifically, regarding the evaluation of vehicle ride quality, a Sperling index of $W \leq 2.5$ is classified as "excellent", while $2.5 < W \leq 2.75$ is classified as "acceptable" (or "qualified"). The calculation formula for the Sperling index is as follows (Eq. 7):

$$W = 3.57 \sqrt[10]{\frac{A^3}{f_v} F(f_v)}, \tag{7}$$

where A is the vibration acceleration (m s^{-2}), f_v is the vibration frequency (Hz), and $F(f_v)$ is the frequency correction factor.

Figure 9 illustrates the distribution of Sperling indices under track irregularity excitations of varying wavelengths. The results demonstrate that, irrespective of vehicle speed, the lateral ride quality trends correlate closely with the sensitive-wavelength distributions previously observed in Figs. 4 and 6. Notably, Condition S5 demonstrates superior efficacy in enhancing lateral ride quality. Across the investigated wavelength and speed regimes, the lateral Sperling index for S5 consistently remains below 2.75, ensuring compliance with stringent ride quality standards. Relative to the

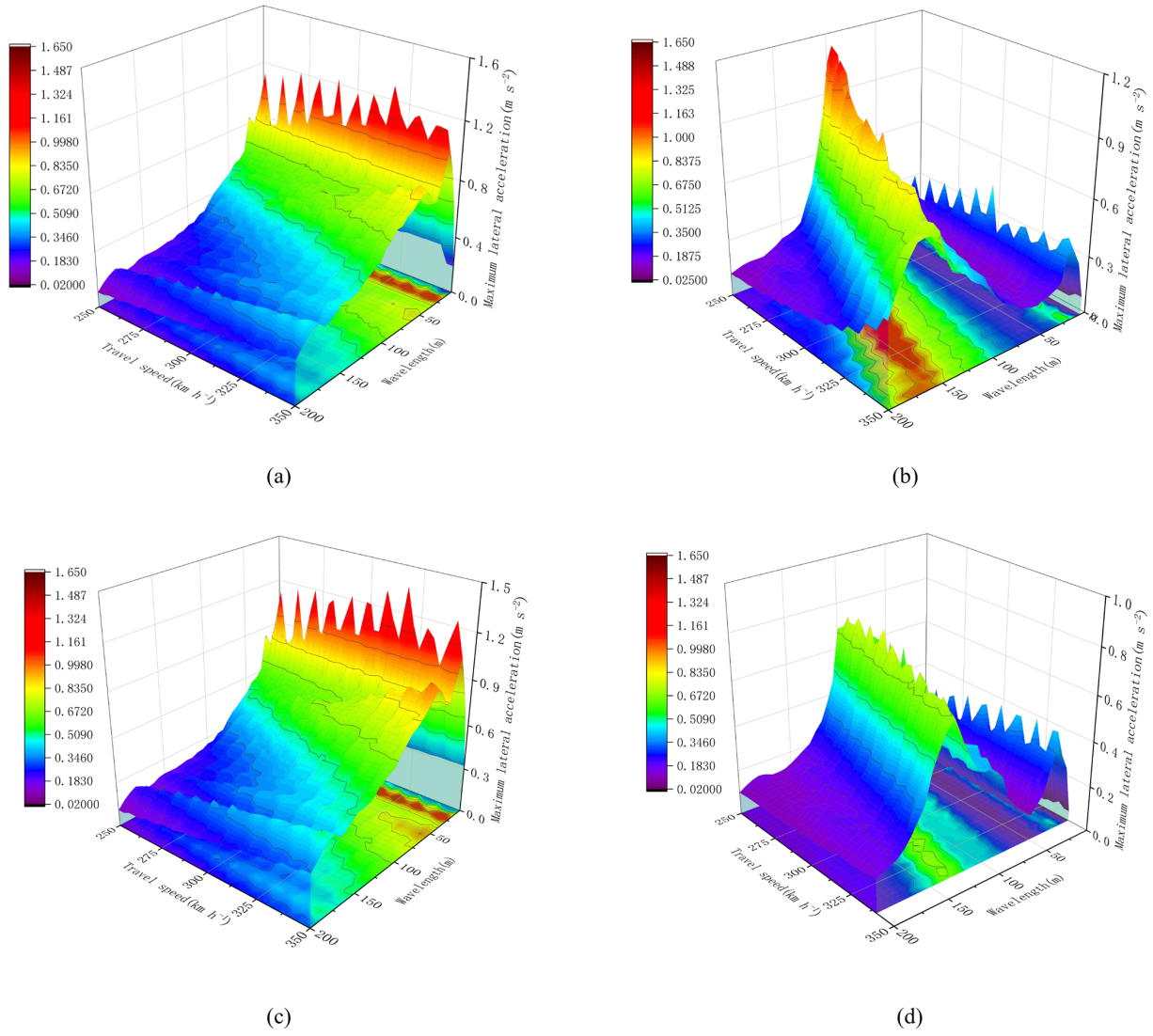

Figure 6. **(a)** Working Condition S2. **(b)** Working Condition S3. **(c)** Working Condition S4. **(d)** Working Condition S5.

baseline (Condition S1), Conditions S5 and S3 achieve index improvements of approximately 28 % and 14 %, respectively. In contrast, Conditions S2 and S4 offer only marginal gains (11 % and 8 %) at sensitive wavelengths, indicating negligible overall enhancement.

5 Coherence validation and result reliability

While the sensitive-wavelength analysis suggests that Condition S5 possesses significant frequency modulation capabilities, statistical validation is required to confirm this efficacy. Accordingly, the coherence function is utilized to quantify the linear correlation between track excitations and the suspension system's response.

The coherence function measures the correlation strength between two random signals in the frequency domain, describing their linear correlation (Sun et al., 2024; Shi et al., 2021). Let the input signal $x(t)$ and the output signal $y(t)$ be two random signals; their coherence function is defined as follows (Eq. 8):

$$\gamma_{xy}^2(\omega) = \frac{|S_{xy}(\omega)|}{S_x(\omega) S_y(\omega)}, \tag{8}$$

where $S_x(\omega)$ and $S_y(\omega)$ are the auto-power spectral densities of $x(t)$ and $y(t)$, respectively; $S_{xy}(\omega)$ is the cross-power spectral density of $x(t)$ and $y(t)$; and ω is the frequency. For all frequencies, the coherence function satisfies $0 \le r_{xy}^2(\omega) \le 1$. When the input $x(t)$ and output $y(t)$ are uncorrelated, $r_{xy}^2(\omega) = 0$; when they are perfectly correlated, $r_{xy}^2(\omega) = 1$. A larger value of $r_{xy}^2(\omega)$ indicates a higher degree of coherence between the input and output, implying that the

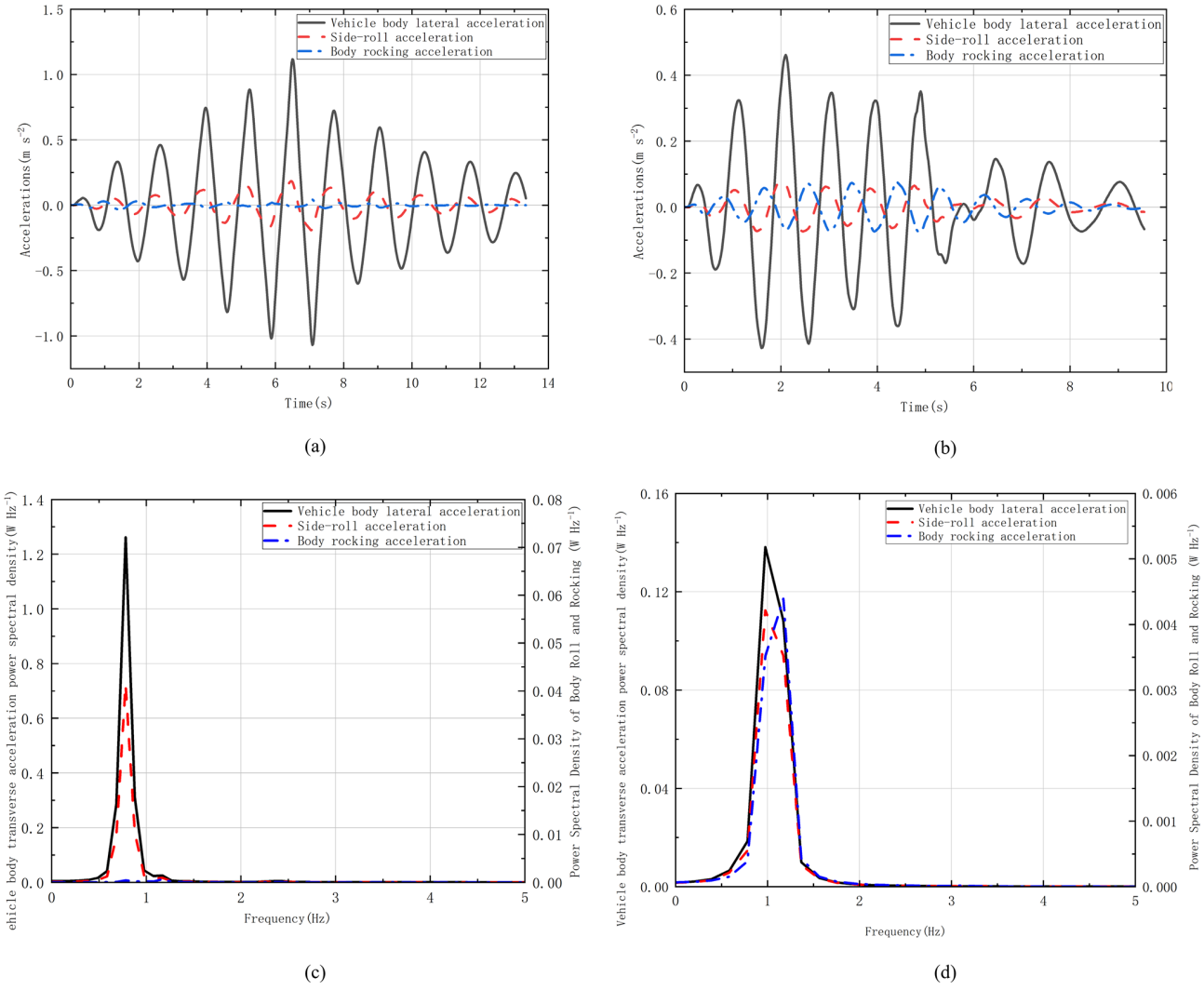

Figure 7. **(a)** Time-domain analysis in resonance state. **(b)** Time-domain analysis in non-resonance state. **(c)** Frequency-domain analysis in resonance state. **(d)** Frequency-domain analysis in non-resonance state.

output response at this frequency is more significantly influenced by the current input excitation.

To investigate the distribution of sensitive wavelengths for lateral track irregularities under various suspension conditions, a random track irregularity model is established. Typically, the wavelength and amplitude characteristics of random irregularities are characterized using frequency response analysis (FRA) combined with the FRA power spectral density factor (FPF) (Shi et al., 2021). To directly bridge the relationship between irregularity wavelengths and the vehicle's dynamic performance, the track irregularity is modeled as harmonic excitation, as expressed in Eq. (9):

$$I_r = A_0 \sin\left(\frac{2\pi x}{\lambda}\right), \tag{9}$$

where A_0 is the amplitude of the harmonic irregularity, x is the distance from the track starting point, and λ is the irregularity wavelength.

Track irregularity is regarded as a stochastic process varying with distance, where its PSD represents the Fourier transform of the autocorrelation function. In this study, data processing and analysis were performed within the MATLAB (R2024a) environment. The PSDs of both the car body lateral acceleration signals and the track irregularity excitations were estimated using the Welch periodogram method, with a Hamming window selected to minimize spectral leakage (Liu et al., 2022). Furthermore, coherence analysis was employed to quantify the correlation strength between track irregularities and vehicle dynamic indices, thereby revealing the sensitivity distribution of the vehicle to irregularities across different wavelengths.

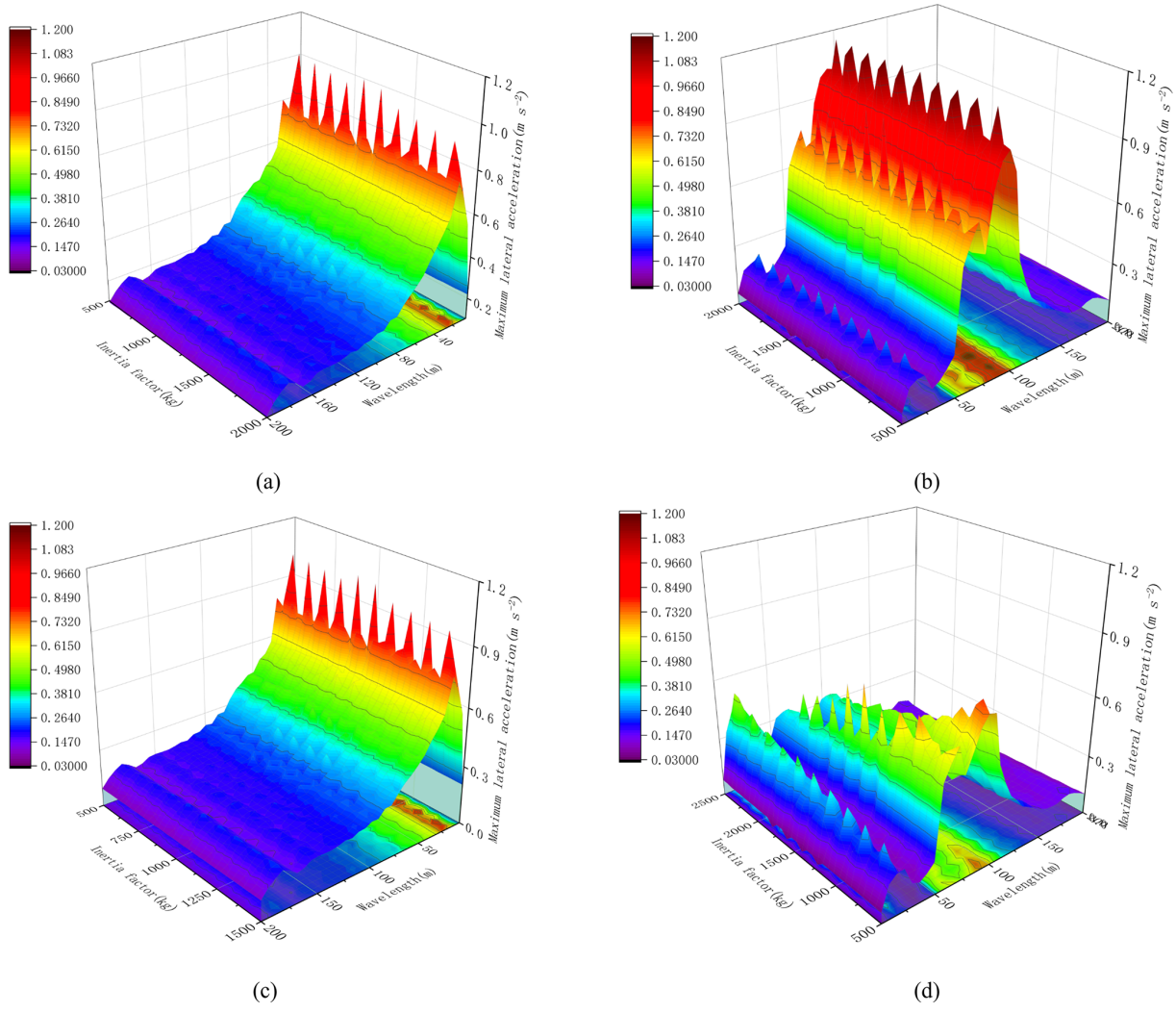

Figure 8. **(a)** Working Condition S2. **(b)** Working Condition S3. **(c)** Working Condition S4. **(d)** Working Condition S5.

Coherence results for each condition

In this study, the FRA algorithm was utilized to synthesize random lateral and vertical track irregularities. With the FPF parameter set to 0.25, the simulation generated lateral irregularities characterized by amplitudes of 4–5 mm across a wavelength range of 5–200 m at a vehicle speed of 250 km h^{-1}. Regarding the identification of sensitive wavelengths, a criterion based on the maximum lateral acceleration power spectrum was adopted: a wavelength is deemed sensitive if it corresponds to a spectral peak that coincides with a significant magnitude in the coherence function (Li, 2022).

Figure 10 depicts the coherence functions and PSD plots relating lateral car body vibration to track irregularities. For Conditions S1, S2, and S4, coherence values exceed 0.8 within the spatial frequency band of 0.04–0.047 m^{-1} (corresponding to wavelengths of 21.1–25 m), identifying sensitive wavelengths of 21.1, 23.3, and 25.5 m, respectively. In contrast, Conditions S3 and S5 demonstrate significant coherence in the low-frequency range of 0.009–0.0092 m^{-1} (wavelengths of approximately 108–111 m), with sensitive wavelengths identified at 110.7 and 107.4 m. These distributions align closely with the sensitive-wavelength results previously established in Fig. 4.

Notably, although the coherence values for Conditions S3 and S5 fall below the 0.8 threshold at sensitive wavelengths, this can be attributed to the specific suspension topology (Fig. 2). In these configurations, the series arrangement of the inerter modifies the lateral-force transmission path. Due to the inerter's inherent mechanical characteristics (Liu, 2023), the system not only attenuates the acceleration amplitude but also elongates the vibration period. This introduces a significant phase discrepancy (or lag) between the car body response and the track excitation, consequently suppressing the calculated coherence values at these wavelengths.

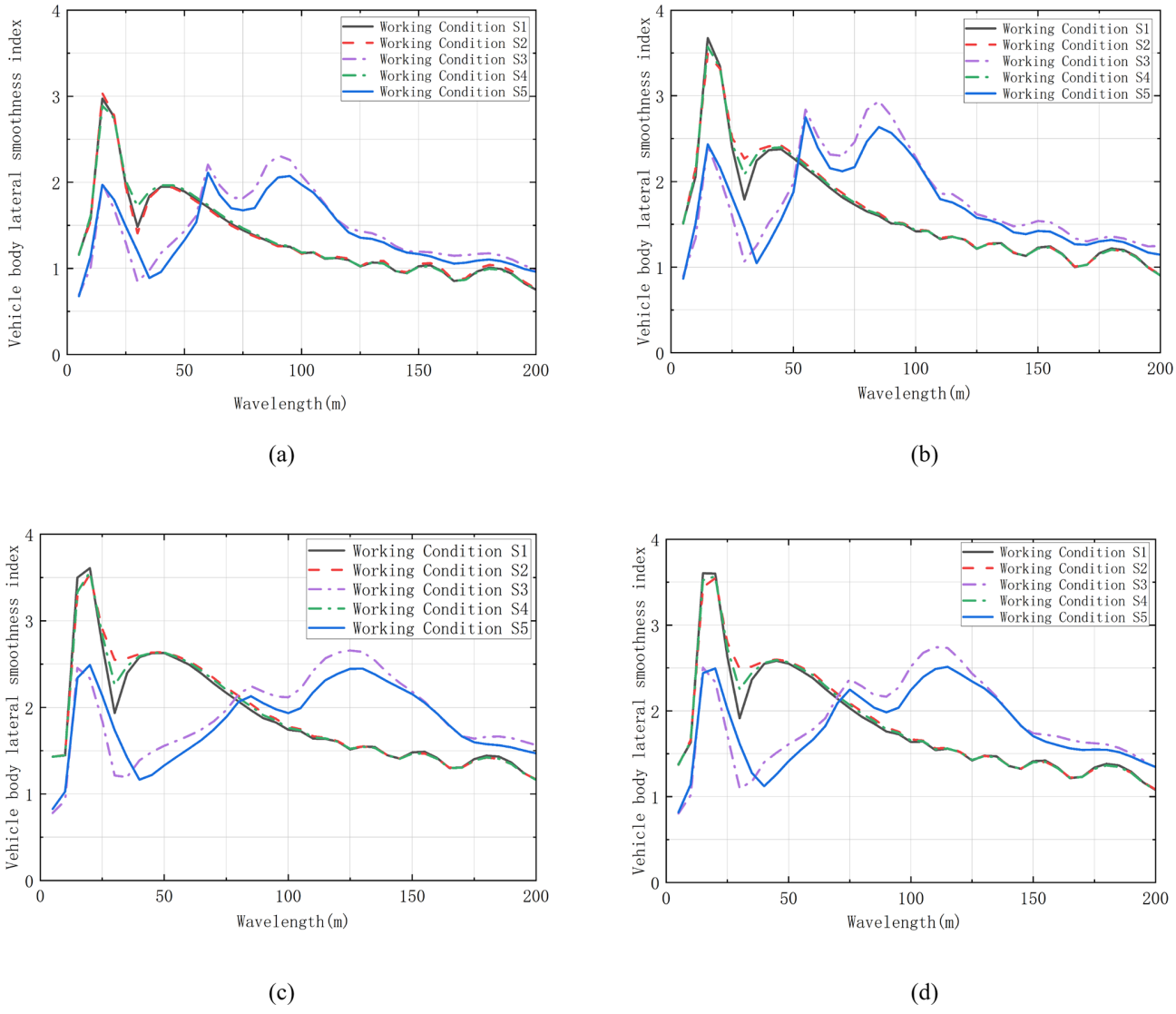

Figure 9. **(a)** Running speed 250 km h^{-1}. **(b)** Running speed 275 km h^{-1}. **(c)** Running speed 325 km h^{-1}. **(d)** Running speed 350 km h^{-1}.

6 Conclusions

This study investigated the impact of diverse inerter-based suspension configurations on sensitive-wavelength distribution and the ride quality of railway vehicles. The results elucidate the distinct vibration attenuation mechanisms of inerters, underscoring their potential for practical engineering applications. Furthermore, the study outlines existing constraints and identifies key avenues for future optimization. The primary conclusions are summarized as follows:

1. All inerter-based configurations (S2–S5) effectively attenuate vehicle vibration under harmonic lateral excitation. S2 and S4 are sensitive primarily to short wavelengths (peaking around 20 m), whereas S3 and S5 target the long-wavelength regime, with acceleration peaks near 105 m.

2. Sensitive wavelengths remain independent of vehicle speed, although peak acceleration generally rises with speed. While varying the inertance coefficient has limited overall impact, configuration S5 uniquely achieves significant suppression with an inertance of 500–1000 kg.

3. Condition S5 (a parallel damper–spring pair in series with an inerter) effectively targets and mitigates the response at the sensitive wavelength of 107.4 m. Under ISO 2631-1, such longwave excitations ($\sim$ 100 m) are identified as major causes of motion sickness and low-frequency environmental pollution. Among the studied cases, Case S5 delivers the optimal attenuation performance, ensuring the ride quality index remains "qualified" or "excellent" throughout the specified range. These results confirm the configuration's practical util-

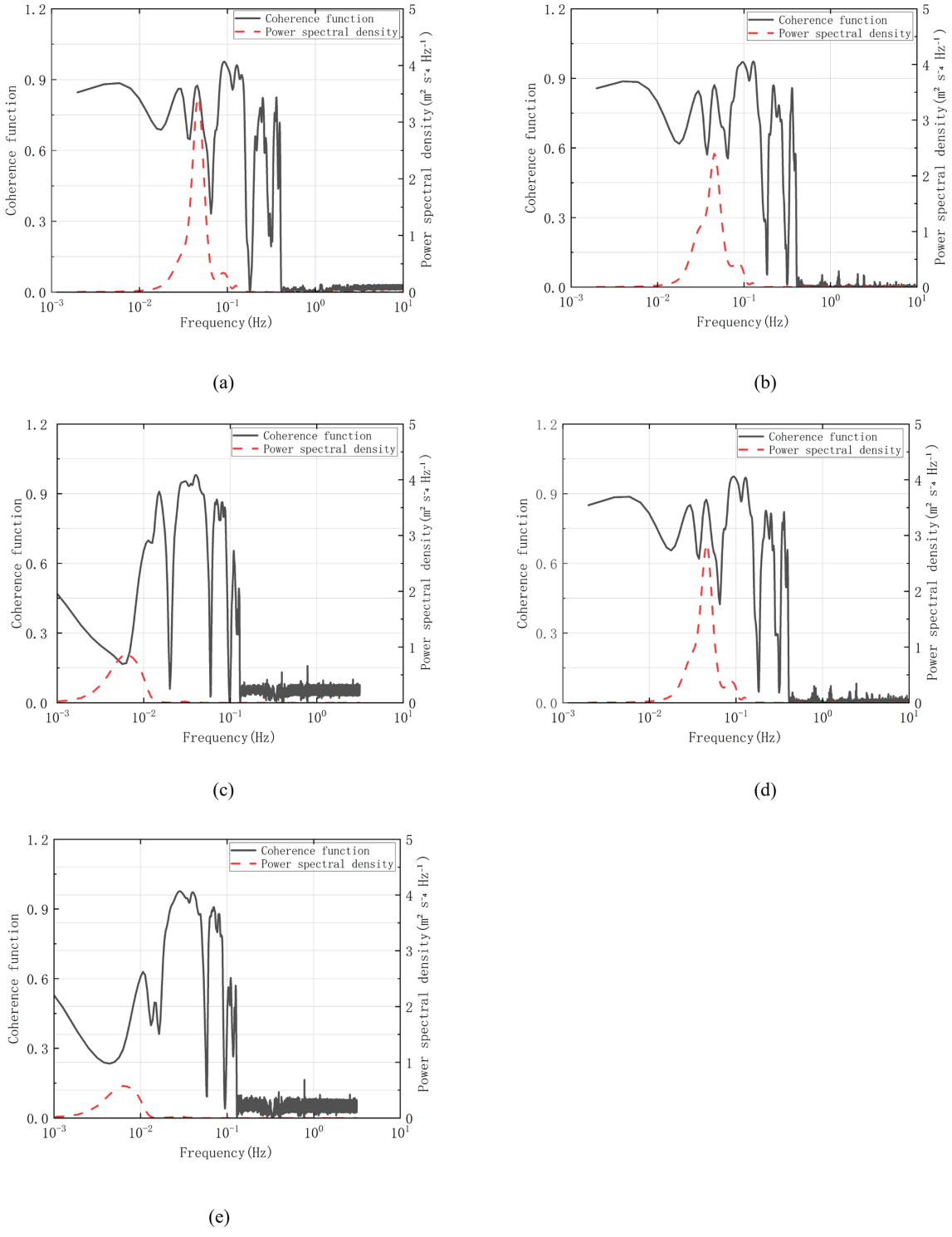

Figure 10. **(a)** Working condition S1. **(b)** Working Condition S2. **(c)** Working Condition S3. **(d)** Working Condition S4. **(e)** Working Condition S5.

ity in eliminating longwave safety risks and improving passenger comfort, validating its high value for engineering applications.

4. Using the coherence function and power spectral density under random track irregularity excitation, sensitive wavelengths for the car body were identified. These were approximately 23.3 m for S2, 25.5 m for S4,

110.7 m for S3, and 107.4 m for S5. These findings align with the results reported in the Conclusions. Critically, this validates the efficacy of Condition S5, characterized by a parallel damper–spring unit in series with an inerter and then in parallel with an air spring, in suppressing longwave track irregularities in railway vehicles.

Certain limitations of this study are acknowledged. First, the multi-rigid-body framework neglects car body flexibility, which may compromise prediction accuracy for high-frequency vibrations induced by short-wavelength irregularities. Second, the analysis is confined to lateral excitations, leaving the coupled effects of vertical irregularities underexplored. Third, the findings rely solely on numerical simulations, lacking validation from scaled bench or field tests. Consequently, future research will prioritize (1) establishing rigid–flexible coupling models to enhance high-frequency prediction fidelity, (2) conducting bench tests and simulations under composite (lateral–vertical) excitations, and (3) developing semi-active inerters for real-time parameter tuning. These initiatives aim to achieve precise "wavelength–speed–parameter" matching, thereby optimizing high-speed-train design for superior ride comfort.

Code availability. The software code used in this study is proprietary and was developed specifically for this research project. Due to intellectual property restrictions, the code is not publicly accessible in a repository. However, the authors are committed to scientific transparency, and the code can be made available by the corresponding author upon reasonable request for the purpose of verifying the results.

Data availability. The underlying research data were obtained from the actual field operations of China's high-speed railway through a cooperation agreement with the relevant railway authorities. These data are subject to strict confidentiality and non-disclosure agreements and contain sensitive information regarding national infrastructure operations. Therefore, the data are not publicly accessible due to third-party restrictions and security protocols.

Author contributions. D. Chen: conceptualization, methodology, writing – original draft. C. Liu: validation, formal analysis, investigation. Z. Xia: resources, data curation, software. C. Huang: writing – review and editing, visualization. R. Zhang: supervision, project administration, funding acquisition. R. Song: supervision, funding acquisition. All authors have read and agreed to the published version of the paper.

Competing interests. The contact author has declared that none of the authors has any competing interests.

Disclaimer. Publisher's note: Copernicus Publications remains neutral with regard to jurisdictional claims made in the text, published maps, institutional affiliations, or any other geographical representation in this paper. The authors bear the ultimate responsibility for providing appropriate place names. Views expressed in the text are those of the authors and do not necessarily reflect the views of the publisher.

Acknowledgements. The authors gratefully acknowledge Mr. Xia from the Locomotive and Car Research Institute for his valuable expertise in rail transportation. We also extend our appreciation to all the specialists who contributed insightful discussions during the experimental phase of this work.

Financial support. This research has been supported by the China Academy of Railway Sciences (grant no. 2024YJ303), the National Natural Science Foundation of China (grant no. 52502482), and the Shanghai Institute of Technology (grant nos. XTCX2024-07 and 101100250099111-A07).

Review statement. This paper was edited by Marek Wojtyra and reviewed by Ján Dižo and three anonymous referees.

References

Alves, H. P. C., Gonzalez, P. R., Raidam, F., and Gerlici, J.: Effect of primary suspension and friction wedge maintenance parameters on safety and wear of heavy-haul rail vehicles, Wear, 524–525, 204812, https://doi.org/10.1016/j.wear.2023.204812, 2023.

Chen, D., Cao, W., Yang, C., and Wu, P.: Investigation of low-frequency lateral abnormal hunting for railway vehicle car bodies, J. Technol. Appl., 22, 263–269, 2022 (in Chinese).

Chen, L., Sun, J., Li, H., and Guo, Y.: Frequency-domain characteristics of vibration response and its relationship with track irregularity wavelength for 400 km h^{-1} high-speed railway vehicles, China Railw. Sci., 46, 157–166, https://doi.org/10.3969/j.issn.1001-4632.2025.01.18, 2025 (in Chinese).

Chen, Z. and Zhu, G.: Semi-active control of subway vehicles based on flexible multi-body dynamics, J. Traffic Transp. Eng., 21, 298–309, https://doi.org/10.19818/j.cnki.1671-1637.2021.06.024, 2021 (in Chinese).

Chudzikiewicz, A., Bogacz, R., Kostrzewski, M., and Konowrocki, R.: Condition monitoring of railway track systems by using acceleration signals on wheelset axle-boxes, Transport, 32, 201–210, https://doi.org/10.3846/16484142.2017.1342101, 2017.

Dižo, J., Blatnický, M., Harušinec, J., Falendysh, A., Melnik, R., and Kostrzewski, M.: Fundamentals of modeling the multibody system of a wagon with a deformable component, in: Proceedings of 23rd International Scientific Conference Transport Means 2019, Palanga, Lithuania, 2–4 October 2019, Part II, 791–796, , ISSN 2351-7034, 2019.

Jiang, P., Liang, L., Xin, D., and Goda, K.: Resonance of railway vehicles induced by floating-slab tracks: mecha-

nism and countermeasures, Veh. Syst. Dyn., 60, 4098–4117, https://doi.org/110.1080/00423114.2021.1995610, 2022.

Kostrzewski, M.: Analysis of the shunting locomotive dynamical characteristics during the ordering work on the hump, Arch. Transp., 44, 31–41, https://doi.org/10.5604/01.3001.0010.6160, 2017.

Kostrzewski, M. and Melnik, R.: Condition monitoring of rail transport systems: A bibliometric performance analysis and systematic literature review, Sensors, 21, 4710, https://doi.org/10.3390/s21144710, 2021.

Li, H.: Study on dynamic characteristics of coupling system of high-speed train body and undercarriage inertial suspension equipment (Master's thesis), Jiangsu University, Zhenjiang, China, https://doi.org/10.27170/d.cnki.gjsuu.2022.000345, 2022 (in Chinese).

Li, S. and Xu, G.: Research on long-wave irregularity sensitive wavelength of high-speed railway at 400 km h^{-1}, Railw. Stand. Des., 66, 50–54, https://doi.org//10.13238/j.issn.1004-2954.202106290006, 2022 (in Chinese).

Li, Z., Sun, Z., Zhang, X., and Wang, Z.: Uncertain frequency response analysis of clamp-pipe systems via the coordinate transformed polynomial chaos expansion, Int. J. Pres. Ves. Pip., 199, 104780, https://doi.org/10.1016/j.ijpvp.2022.104720, 2022.

Liu, K.: Study on dynamic characteristics and application of composite nonlinear vibration isolation system with inerter (Master's thesis), Lanzhou Jiaotong University, Lanzhou, China, 2023 (in Chinese).

Qi, Y., Ao, P., Dai, H., Jiang, Y., and Wang, K.: Study on lateral stability of a high-speed EMU bogie with elastic frame suspension of inerter, J. Vib. Shock, 44, 65–72, https://doi.org/10.13465/j.cnki.jvs.2025.02.009, 2025a (in Chinese).

Qi, Y., Li, W., Liu, Z., Jiang, Y., and Wang, K.: Sensitivity wavelength analysis of track geometric irregularities for subway vehicle hunting, China Mech. Eng., 36, 1–9, https://doi.org/10.3969/j.issn.1004-132X.2025.05.004, 2025b (in Chinese).

Sharma, K. S., Sharma, R. C., Choi, Y., and Jung, H.-S.: Experimental and mathematical study of flexible–rigid rail vehicle riding comfort and safety, Appl. Sci., 13, 5252, https://doi.org/10.3390/app13095252, 2023a.

Sharma, K. S., Sharma, R. C., Choi, Y., and Jung, H.-S.: Modelling and dynamic analysis of adaptive neuro-fuzzy inference system-based intelligent control suspension system for passenger rail vehicles using magnetorheological damper for improving ride index, Sustainability, 15, 12529, https://doi.org/10.3390/su151612529, 2023b.

Shi, H., Luo, R., and Zeng, J.: Review of dynamic evaluation standards for high-speed trains at home and abroad, J. Traffic Transp. Eng., 21, 36–58, https://doi.org/10.19818/j.cnki.1671-1637.2021.01.004, 2021 (in Chinese).

Smith, M. C.: Synthesis of mechanical networks: the inerter, IEEE Trans. Automat. Contr., 47, 1648–1662, https://doi.org/10.1109/TAC.2002.803532, 2002.

Sowiński, B., Stelmach, A., and Chudzikiewicz, A.: Simulation analysis of the influence of changes in track parameters on running safety of a rail vehicle, Energies, 14, 5882, https://doi.org/10.3390/en14185882, 2021.

Sun, W., Wang, J., Thompson, D., and Gong, D.: Vibration fatigue failure analysis of primary coil springs in railway vehicles, J. Vib. Shock, 43, 230–236, https://doi.org/10.13465/j.cnki.jvs.2024.08.027, 2024 (in Chinese).

Sun, Y., Zhou, J., Gong, D., and Ji, Y.: Study on multi-degree of freedom dynamic vibration absorber of the car body of high-speed trains, Mech. Sci., 13, 239–256, https://doi.org/10.5194/ms-13-239-2022, 2022.

Tian, G. Y.: Study on the power spectral density of track irregularities and its relationship with ride quality in high-speed railway (Master's thesis), Southwest Jiaotong University, Chengdu, China, 2015 (in Chinese).

Wang, D.: Research on inertial suspension parameters in vehicle vertical vibration system (Master's thesis), Changzhou University, Changzhou, China, 2023 (in Chinese).

Wang, Y., Li, H., Jiang, W., and Zhou, J.: Research on dynamic characteristics of inertial suspension equipment under high-speed rail vehicle, J. Vib. Shock, 41, 246–254, https://doi.org/10.13465/j.cnki.jvs.2022.02.034, 2022 (in Chinese).

Wei, X. and Xu, G.: Analysis of influence of track irregularity with different sensitive wavelengths on operation performance of modern tram, Sci. Technol. Eng., 21, 13497–13504, https://doi.org/10.3969/j.issn.1671-1815.2021.31.039, 2021 (in Chinese).

Xu, L., Mao, M., Chen, Y., Du, F., and Dai, J.: Overview of design methods for vehicle inerter-spring-damper suspension configuration, Acta Armamentarii, 41, 822–832, https://doi.org/10.3969/j.issn.1000-1093.2020.04.021, 2020 (in Chinese).

Yu, P., Li, J., Zhou, D., and Zhang, K.: Inhibition method of maglev track irregularity on suspension system, J. Natl. Univ. Def. Technol., 38, 191–198, https://doi.org/10.11887/j.cn.201602030, 2016 (in Chinese).

Zhu, H., Zeng, Q., Wang, Y., and Yan, Y.: Research progress on dynamic performance of high-speed trains, J. Traffic Transp. Eng., 21, 57–92, https://doi.org/10.19818/j.cnki.1671-1637.2021.03.005, 2021 (in Chinese).

Zhuang, C., Wushizi, X., and Zhang, Y.: Study on damping effect of inerter-spring-damping device on isolation structure under extreme earthquake, J. Vib. Shock, 38, 112–117, https://doi.org/10.13465/j.cnki.jvs.2019.03.017, 2019 (in Chinese).